Maximization of performance in multi-tube latent heat storage – optimization of fins topology, effect of materials selection and flow arrangements

Pizzolato, Alberto; Sharma, Ashesh; Ge, Ruihuan; Maute, Kurt; Vittorio, Verda; Sciacovelli, Adriano

DOI:
10.1016/j.energy.2019.02.155

Maximization of performance in multi-tube latent heat storage – Optimization of fins topology, effect of materials selection and flow arrangements

Alberto Pizzolato[a], Ashesh Sharma[b], Ruihuan Ge[c], Kurt Maute[d], Vittorio Verda[a], Adriano Sciacovelli[c]*

a Department of Energy, Politecnico di Torino, Corso Duca degli Abruzzi 24, Turin, Italy
b National Renewable Energy Laboratory, Golden, CO, USA
c Birmingham Center for Energy Storage (BCES), School of Chemical Engineering, University of Birmingham, UK
d Department of Aerospace Engineering Sciences, University of Colorado at Boulder, Boulder, CO, USA
* Corresponding author. Email: a.sciacovelli@bham.ac.uk; Tel. +44 (0)121 414 8747;

Abstract

This paper addresses the need of multi-tube latent heat thermal storage (LHTES) systems with enhanced heat transfer performance. Uniquely, this work draws from topology optimization method for thermal energy storage to search for the optimal configuration of fins in multi-tube LHTES systems with different phase change materials (PCMs), flow arrangements and design constraints. The design freedom of topology optimization allows the discovery of innovative LHTES designs and elucidate the link between design and physical processes occurring during charging/discharging. Three key results of this study are: i) the optimized fin design is tightly connected to the type of storage duty cycle, which demonstrates the necessity to account for realistic operating conditions in the optimization process. ii) The fin material should be chosen in parallel with the layout of the fins and not sequentially as commonly done; this indicates that the optimization of LHTES systems is a co-design challenge. iii) Topology optimized multi-tube LHTES units surpass in performance fins optimized for a single-tube configuration in a multi-tube unit. Finally, this work demonstrates for the first time the manufacturability of topology-optimized LHTES units by using 3D printing.

Nomenclature

c_{mat}	specific material cost per unit volume
C_k	PCM-to-HCM diffusivity ratio
C_{TOT}	total cost
E	dimensionless energy
f	liquid fraction
$\boldsymbol{F}$	dimensionless momentum source
$\boldsymbol{g}$	gravity vector
K	dimensionless diffusivity
L	dimensionless latent heat
$\boldsymbol{n}$	normal vector
p	dimensionless pressure
Pr	Prandtl number
t	dimensionless time
T	dimensionless temperature
$\boldsymbol{v}$	dimensionless velocity
V	volume
$\boldsymbol{x}$	dimensionless coordinate

Greek symbols

α	diffusivity
Γ	design domain boundary
ρ_s	"density" field (physical design variable)

Φ_{MAX} maximum volume fraction of HCM

Subscripts

b	Brinkmann
d	Dirichlet
f	final
fc	fully charged
L	latent
m	melting
N	Neumann
NC	natural convection
tot	total

Acronyms

BDF	Backward Differentiation Formula
CFD	Computational Fluid-Dynamics
GCMMA	Globally Convergent Method of Moving Asymptotes
HCM	High Conducting Material
HEX	Heat EXchanger
HTF	Heat Transfer Fluid
LHTES	Latent Heat Thermal Energy Storage
NTU	Number of Transfer Units
PCM	Phase Change Material
PDE	Partial Differential Equation
SoC	State of Charge
STL	STereoLithography
TES	Thermal Energy Storage

1. Introduction

In recent years the roles, benefits and value of thermal energy storage (TES) technologies have dramatically increased under the pressure of supplying clean heat and cold. Final energy consumption for heating and cooling lies between 40-60% in most of the countries [1] and its decarbonization represents a paramount challenge in the view of meeting CO_2 reduction targets, as well as achieving a clean economic growth [2,3]. In this context, TES provides unique flexibility including the reduction of heat and electricity peak demand, use of renewable heat, high efficiency process integration and power-to-heat, enabling clean heating and cooling [4–6]. Under such increasing need for flexibility, it has become evident that fit for purpose TES systems are needed to ensure that they suit the services they intend provide [7–12]. However, the lack of appropriate design methods often hinders the ability to conceive appropriate designs of TES systems.

Shell-and-tubes latent heat thermal storage (LHTES) systems are distinguished from other LHTES configurations by their high compactness, large heat transfer area, and easy integration into thermal processes, which makes it one of the most promising for TES applications. Evidently, the development of shell-and-tubes LHTES systems have significantly drawn from the vast technical knowledge on shell-and-tube heat exchangers (HEXs), which has led to designs consisting of multi-tube passages for the heat transfer fluid (HTF) and PCM filling the shell side [8,13,14]. However, HEXs and LHTES systems differ in three crucial aspects: i) LHTES delivers two processes

over time, i.e. charging and discharging, while HEXs deliver a fixed thermal power near design operating condition; ii) the heat transfer in LHTES is usually dominated by conduction and natural convection [15], while HEXs commonly take advantage of forced convection; iii) the thermal resistance in LHTES varies during charging/discharging due to moving melting/solidification front in the PCM [16], while conventional HEXs show nearly constant thermal resistance. Hence, the simple adoption of HEXs designs for TES systems may severely compromise functionality as well as performance.

Traditional HEXs design optimization methods for LHTES systems do not allow to fully address the three key distinguishing features of LHTES mentioned above, precluding the identification of genuine fit for purpose LHTES configurations. Most of the studies in both academia and industries have in fact relied on a) traditional quasi steady-state design approaches such as the effectiveness-NTU method [17,18], b) parametric analyses in combination with CFD simulations [19,20] and c) lumped parameter models for parametric optimization [21]. As a result, attempts to identify optimized shell-and-tubes LHTES systems have primarily led to traditional solutions, mainly consisting of conventional extended heat transfer surfaces (e.g. fins) on the PCM side of the LHTES system. Some attempts – although limited in scope – have been made to overcome these limitations, for example branched heat transfer enhancement structures [7], and asymmetric configurations [22]. These works attempted to identify, although heuristically, configurations of shell-and-tubes LHTESs capable to achieve optimal charging/discharging process. That is, optimality on the complete time evolution of the system. However, the design approaches commonly adopted lack generality as well as design freedom. Recently [15,23], we demonstrated the use of topology optimization as a systematic approach to find configurations of finned LHTES systems capable to deliver optimized time evolution of charging/discharging processes. Although these studies demonstrated high potential for design-driven innovations in the LHTES technology, they considered single-tube configurations, which are popular only for lab-scale or small facilities.

Most of commercial installations consists of multiple tubes immersed in a unique shell, featuring superior compactness and heat transfer area as compared to single-tube units. Furthermore, multi-tube systems are ideal for applications requiring two separate hydraulic loops, one for the hot and the other for the cold heat transfer fluid (HTF). This configuration is often a necessity in thermal applications, including TES. Separate loops, for example, avoid contact/contaminations between HTFs and allows distinct operating conditions, such as flow rate and pressure. The latter is, for example, a practical requirement for TES applications in district heating TES, where the primary HTF loop (network) is separate from secondary HTF loop (user) [24]. Despite these advantages, the design of multi-tube units received little attention and key design issues remain open. First, although a popular approach to analyze multi-tube systems consists in extending single-tube results exploiting the assumption of periodicity [25,26], it is not clear to what extent this method is valid for design studies. Second, to the best of our knowledge, no previous research ever investigated whether fins optimized for a single-loop operation are a convenient choice for units with multiple loops. Finally and most importantly, the current literature does not provide any indication on how the materials choice and the optimal fin designs are interconnected.

This paper covers all these literature gaps and deals with the optimal design of shell-and-tubes multi-tube LHTES systems with different flow arrangements, phase change materials (PCMs) and high conductivity fin materials. The previous key design questions are answered with matchless design freedom, drawing uniquely from topology optimization method for TES [15,23]. This approach yields: (i) fit for purpose shell-and-tubes LHTESs that surpass conventional LHTES designs and (ii) useful guidelines for design engineers. Finally, the complex optimized geometries are 3D printed to demonstrate the feasibility of the manufacturing process and further reduce the gap with practical applications.

2. Topology optimization of shell-and-tubes LHTES units

Topology optimization responds to the fundamental question of engineering design: how shall we distribute the material in a specific region to obtain a device with maximum performance? The key feature that distinguishes this method from the alternative design routes is the design model, i.e. how the geometry is described by the set of design variables. Many design model flavors have been developed for topology optimization [27], all of them feature superior design freedom as compared to conventional size and shape optimization methods. They allow the simulteanous optimization of the size, shape, number and connectivity of both void and material domains. The design freely evolves throughout the optimization process, often leading to non-intuitive configurations. The method was developed by the structural community nearly three decades ago [28,29] and has been widely employed within the aerospace and automotive industries for weight and cost reduction of mechanical parts [30]. The recent advances of Additive Manufacturing (AM) technologies are giving new momentum to this design methodology which is rapidly expanding in the energy field, for the design of e.g. thermoelectric components [31], Li-Ion batteries [32] and LHTES units [15,23].

Following our previous contributions [15,23], in this paper we control the geometry using a density approach. The layout of highly conductive fins within the shell domain is represented by an element-wise constant spatial distribution, generally referred to as "density field". It intuitively corresponds to the volume fraction of the Highly Conductive Material (HCM). The values of the density field are bounded between zero and one, with one denoting pure HCM and zero denoting pure PCM. This density field is generally labeled as ρ_s. We aim at minimizing the final time, t_f, required for a complete charge or discharge. These processes are considered complete when the energy in the unit, E, reaches 95 % and 5 % of the total capacity in fully-charged conditions, E_{fc}. The amount of HCM volume utilized, V_{HCM} needs to be constrained since, without an upper bound, the optimization process would return a trivial solution comprising of full HCM, i.e. a unit with negligible storage capacity. Hence, we prescribe a maximum volume fraction, Φ_{MAX}, of HCM within the shell domain. Formally, the optimization problem can be stated in mathematical terms as follows:

$$\begin{aligned} \underset{\rho_s}{\text{minimize}} \quad & t_f \\ \text{s.t.} \quad & E(t_f) - SoC(t_f) E_{fc} = 0 \\ & V_{HCM} - \Phi_{\mathrm{MAX}}\, \mathrm{V_{tot}} \leq 0 \end{aligned} \tag{1}$$

where SoC indicates the State of Charge and V_{tot} the total volume of the unit.

To solve the optimization problem (1), our systematic framework needs to compute the physical response of the system. As in [15], we model phase change through a fixed-grid method that does not require to track explicitely the melting front. We adopt the following dimensionless version of the incompressible Navier-Stokes equations:

$$\frac{\partial v_i}{\partial x_j} = 0 \tag{2}$$

$$\frac{\partial v_i}{\partial t} + v_j \frac{\partial v_i}{\partial x_j} = -\frac{\partial p}{\partial x_i} + Pr \frac{\partial}{\partial x_j}\left(\frac{\partial v_i}{\partial x_j} + \frac{\partial v_j}{\partial x_i}\right) + F_{NC} + F_L + F_{b_i}(\rho_s) \tag{3}$$

$$\frac{\partial T}{\partial t} + v_j \left(1 + L(\rho_s)\frac{\partial f}{\partial T}\right)\frac{\partial T}{\partial x_j} = \frac{\partial}{\partial x_j}\left(K(p_s)\frac{\partial T}{\partial x_j}\right) - L(\rho_s)\frac{\partial f}{\partial t} \tag{4}$$

where x_i is the dimensionless spatial dimension, t is the dimensionless time, v_i is the dimensionless velocity, p is the dimensionless pressure, T is the dimensionless temperature, f is the liquid fraction and Pr is the Prandtl number. The third and fourth terms on the RHS of the momentum equation, F_{NC} and F_L, correspond to the contributions of natural convection and phase change, respectively. Design modifications are accounted for within the physical model through three design-depentent terms: a Brinkmann sink in the momentum equation, $F_{b_i}(\rho_s)$, the dimensionless latent heat in the energy equation, $L(\rho_s)$, and the dimensionless diffusivity in the energy equation, $K(\rho_s)$. The latter are used to make the material properties distributions consistent with the layout the

HCM and PCM domains. For instance, the term $F_{b_i}(\rho_s)$ acts as a momentum sink of tunable magnitude, suppressing the velocities in those areas occupied by HCM and yielding no contribution in those areas occupied by PCM. To reduce the computational complexity of the analysis model, we exploit symmetry and consider only half of the shell (Figure 1).

The complete PDE problem is constructed considering a set of time-independent boundary conditions and space indepent initial conditions. We prescribe an adiabatic boundary on the external shell Γ_{N_1} and a symmetry boundary condition on Γ_{N_2} such that:

$$K(\rho_s)\frac{\partial T}{\partial x_i}n_i = 0 \qquad on\ \Gamma_{N_1} \cup \Gamma_{N_2} \quad (5)$$

The temperature is fixed at the internal boundary, Γ_d, to represent the contact with the tube containing the heat trasfer fluid (HTF):

$$T = T_d \qquad on\ \Gamma_d \quad (6)$$

where $T_d = 1$ for charge and $T_d = 0$ for discharge. The momentum interaction with the external shell and pipe boundaries is modeled using a no-slip condition (on $\Gamma_{N_1} \cup \Gamma_d$). Due to symmetry, non-penetration and vanishing tangential stresses are prescribed on Γ_{N_2}. To obtain a well-posed incompressible Navier-Stokes problem in the enclosure, the pressure $p = 0$ is specified at point A. This choice does not modify the thermal and fluid-dynamic responses. The state variable fields are initialized with $v_i = 0$, $p = 0$ and $T = T_I$, with T_I denoting the initial temperature field, which is set to 0 and 1 for charge and discharge, respectively.

The optimization problem is solved using the Globally Convergent Method of Moving Asymptotes (GCMMA) [33], an efficient gradient-based optimization routine tailored for topology optimization problems. To simplify sensitivity analysis, the binary representation of the design presented in this section is relaxed to a continuous [0, 1] density distribution and special interpolation laws for the design-dependent terms $F_{b_i}(\rho_s)$, $L(\rho_s)$ and $K(\rho_s)$ are formulated [23]. To avoid numerical instabilities, we introduce a nodal design variable field. The element-wise density field, ρ_s is computed through filtering and projection [34], as discussed in [23]. The governning PDEs are discretized in space using ~15k four-node bilinear quadrilateral finite elements. The time stepping relies on a fully implicit first-order Backward Differentiation Formula (BDF) and an adaptive scheme [35]. The system of nonlinear equations arising at each time-step are solved using a damped Newton solver. The resulting analysis framework was verified and validated in [15]. For further details about the numerical implementation, we refer the reader to our previous work [15].

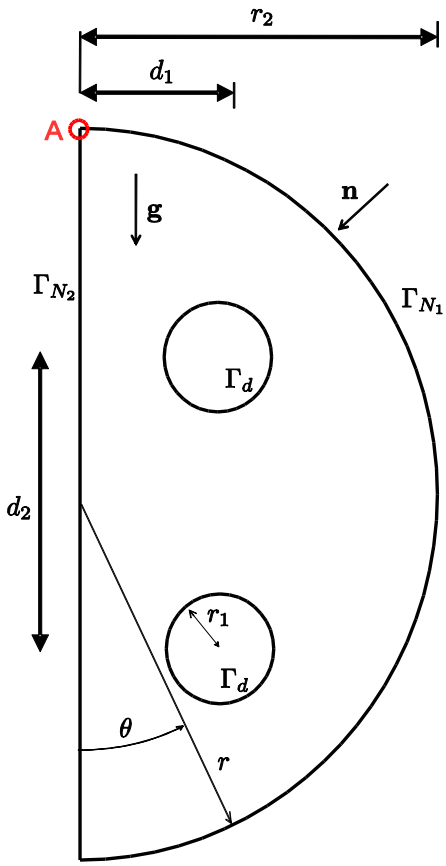

Figure 1. Schematic of the design domain.

3. Results and Discussion

3.1. Optimal design of fins for conduction dominated and convection dominated shell-and-tubes LHTES units

Multi-mode heat transfer (conduction and convection) is well known to significantly affect the performance of LHTES units. Past studies have in fact clearly pointed out that, as a general guideline, discharge is largely conduction dominated due to suppression of natural convection in the liquid PCM [10,36]. On the other hand, charging process is enhanced by natural convection currents. Namely, faster melting is due to the enhancement in heat transfer within the LHTES caused by natural convection. This could potentially introduce a severe difference between the charging process (PCM melting in our case) and the discharge process (PCM solidification). Therefore, we address how the optimized design of shell-and-tubes LHTES units is affected by such an intrinsic difference in the underlying physical phenomena by taking advantage of the capabilities of the topology optimization method.

It is worthy to notice that for finned LHTES units – which is the case here – the predominance of conduction or convection is not solely dependent on the PCM, but also on the amount and type of HCM and on the fin layout. As HCM is highly thermally conductive, it obviously enhances heat conduction. Furthermore, the presence of HCM fins may prevent the formation of strong convective currents. These two factors might lead to conduction dominated cases even in the case of charging processes. Therefore, we defined $C_k = \alpha_{PCM} / \alpha_{HCM}$ as the PCM-to-HCM thermal diffusivity ratio, and we explored the optimized designs across a spectrum of different values C_k to identify conduction or convection dominated layouts. All remaining physical parameters were set as in our

previous paper [15], while the volume of HCM was set to 10 % of the total available. The design domain has dimensions $r_1 = 0.125$, $r_2 = 1$, $d_1 = 0.35$, $d_2 = 0.7$ (see Fig. 1).

Fig. 2 illustrates the topology optimization process by showing the evolution of the HCM layout at different optimization iterations for a case with convection deliberately deactivated in our model. The initial design (iteration 0) corresponds to a homogeneous density distribution, $\rho_s = \Phi_{MAX}$. During the first 20 iterations, HCM concentrates in a region close to the HTF pipes. Then, at iteration 60, gray ramification patterns start to appear, which are gradually converted into a black-and-white layout. The final optimized geometry is obtained after 134 optimization iterations. The same optimized design is found for both charging and discharging, as there are no differences between the two processes. The optimized layout of Fig 2 is evidently symmetric with respect to both vertical and horizontal planes, with the layout of fins identical for each pipe. This reveals that such optimized design aims for uniform enhancement of heat conduction throughout the entire domain, without any preferential directions. The branches of the fins stretch mainly toward the outer shell of the LHTES unit. This is where heat transfer enhancement is needed most, particularly for deep charge/discharge of the system. In such a case, the last fraction of PCM to melt/solidify is situated near the wall of the shell, which requires fins oriented toward those areas of the unit.

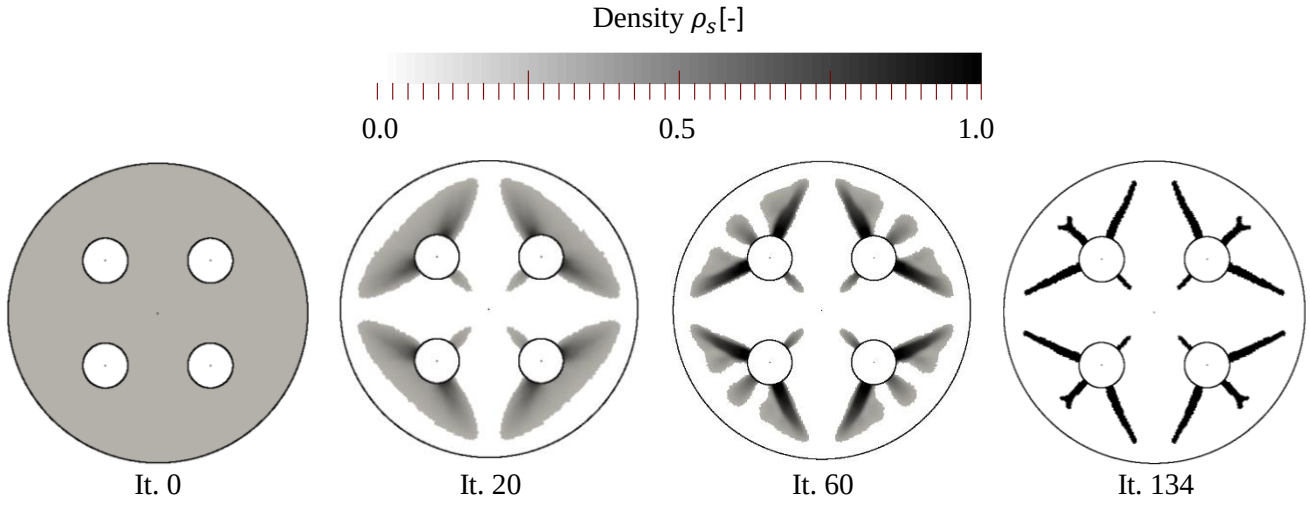

Figure 2. Evolution of conduction-dominated design at selected iterations along the topology optimization process.

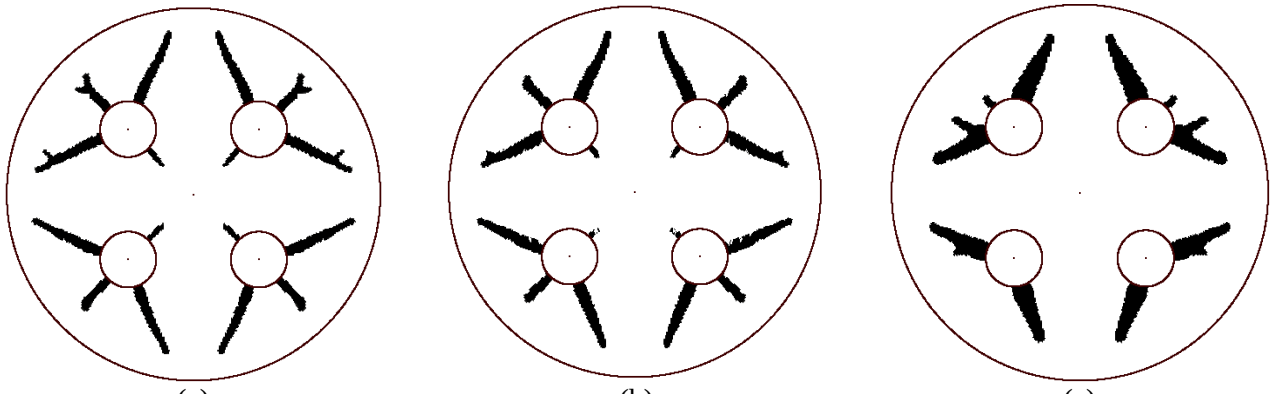

Figure 3. Optimized designs for solidification with (a): C_k= 1 %; (b) C_k = 2 %; (c): C_k=5 %.

As the PCM-to-HCM thermal diffusivity C_k increases, the relative impact of natural convection becomes relevant, which reverberates as well on the optimized LHTES configuration. Figure 3 illustrates the designs optimized for discharge process (PCM solidification) and for C_k = 1%, 2% and 5%. Natural convection was accounted in our model and the results were compared with the limiting case presented in Fig 2. For C_k = 1% the configuration of the fins appears nearly identical to the one found the in the limiting case of Fig. 2. As C_k increases, the configurations (Fig 3a and Fig 3b) do not shows substantial modifications, with the fins still mainly oriented outwards toward the external shell. Only design (c) presents thicker fins but no net changes in orientation and topology are observed. The similarity between the designs (Figs 3a-c) is a testament that PCM solidification (discharge process) remains largely dominated by pure heat conduction, leading to alike optimized designs.

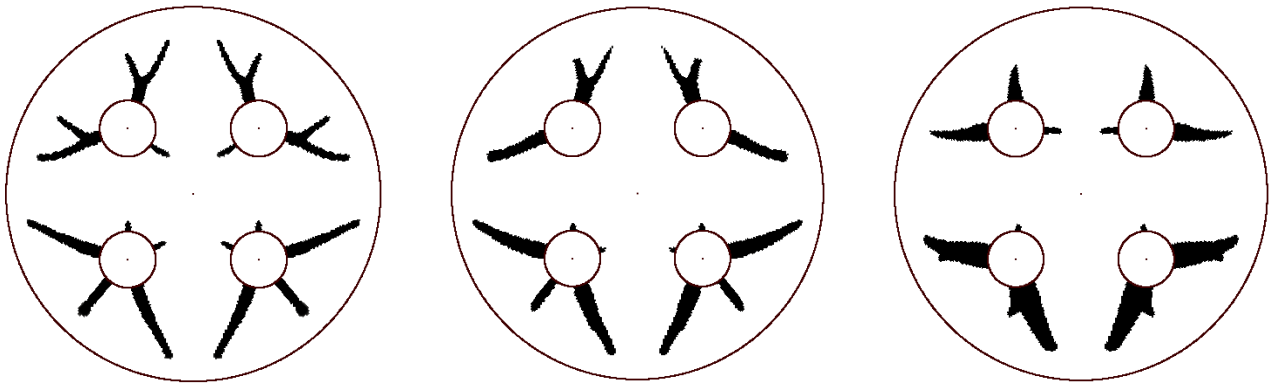

(a) (b) (c)

Figure 4. Optimized designs for melting with (a): C_k= 1 %; (b) C_k = 2 %; (c): C_k=5 %

The results change quite drastically when PCM melting (charging) is considered, as illustrated in Fig 4. A cursory comparison between Fig 3 (solidification) and Fig 4 (melting) indicates that asymmetrical fins are favorable for the PCM melting process, which is a first indication that natural convection plays a role here. For C_k = 5 % (Fig 4c), the fins surrounding the top tube are short structures with different orientation. Short fins elements elongate toward the top region while large and thick ones from the bottom pipes are oriented toward the lower portion of the unit. Note that, although designs optimized for charging and discharging are different, the amount of PCM and HCM in the tank is equal because: (i) both layouts are optimized with the same Φ_{MAX} in Eq. (1) and (ii) the inequality constraint is active. This consideration holds for all the numerical examples presented in the remainder of the paper. Further insights into these designs can be obtained by considering the PCM liquid fraction.

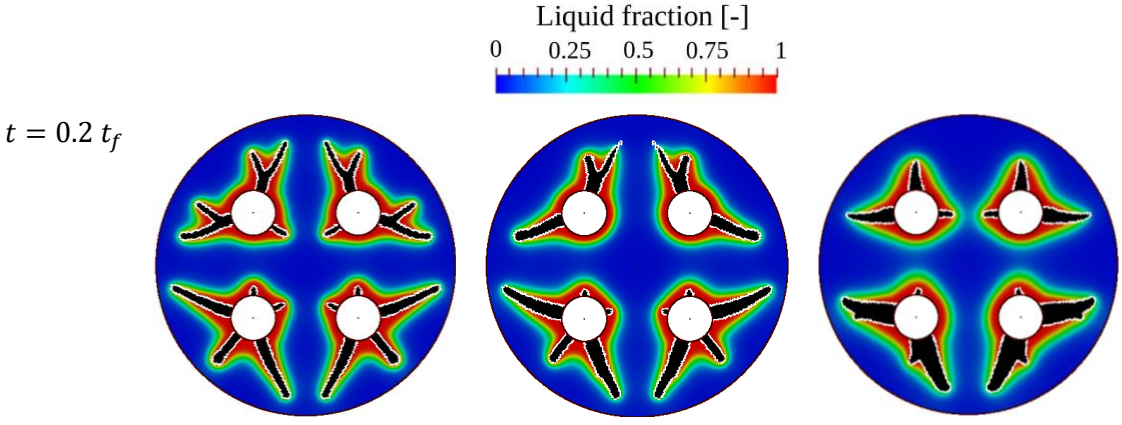

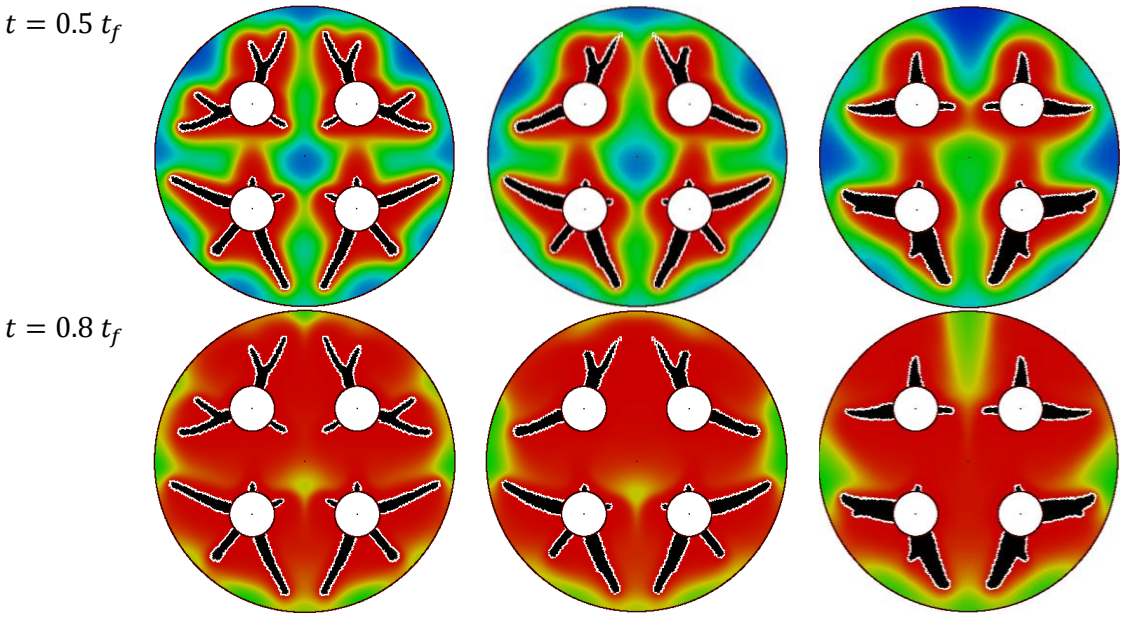

Figure 5. Liquid fraction during melting at selected fraction of the final process time, t_f. Referring to Figure 4, the left column shows design (a), the central column shows design (b), the right column shows design (c)

The time evolution of the liquid fraction field, as represented in Fig 5, sheds a light on the melting process and the heat transfer enhancement brought by the optimized fins. In particular, the shape of the melting front highlights how the designs exploit different strategies to melt the PCM. That is, how the benefit of natural convection is exploited to promote the charging process. From Fig 5, until 20% of the process no relevant differences can be observed: melt fronts initiate very similarly along the fins of each of the four pipes. At 50%, asymmetries between the melting front for the top and bottom pipes start to appear. Driven by buoyancy, liquid PCM starts to flow upwards from the bottom two pipes. Consequently, the bottom melting front begins to merge with the one from the upper two pipes. Such phenomenon is far more evident for design (c), which is a consequence of the larger role played by convective heat transfer in this case, as suggested by the higher C_k (C_k = 5%).

An in-depth look at the liquid fraction fields also elucidates the role played by the optimized fins and it explains their overall shape. In design (c), fins oriented upward are almost completely absent, indicating that minimal heat transfer enhancement is required along such direction. This is due to the strong natural convection, which intrinsically enhances heat transfer in the top part of the LHTES unit. Therefore, the role of the optimized fins is to ensure good heat transfer in the lower part of the LHTES unit, where PCM melting does not benefit from natural convection. It is interesting to notice that in design (c) of Fig 5 two short vertical branches appear on the upper pair pipes, while the same feature is absent for the two bottom pipes. Such two branches provide a minimal enhancement of heat transfer in the top part of the unit needed to counterbalance the effect of the two upper pipes on the advancement of the melting front. As illustrated before, a melt front departs from the bottom two pipes and moves upward due to convection. Such front advancement is obviously obstructed by the surfaces of the upper pair of pipes, hence reducing the enhancement of PCM melting in the very upper shell region (above the upper pair of pipes) – such enhancement is provided by the short two vertical branches. Such reason is further reinforced by the evident fact that in Fig 5 design (c) no branches of the fins are oriented toward the center of the LHTES unit; here is where the enhancement caused by convection is maximum. Hence, no highly conductive material is needed in this region.

3.2. Effect of the periodicity assumption on the optimizedl designs of shell-and-tubes LHTES units

A common approach followed in the literature consists in designing and optimizing shell-and-tubes LHTES units under the assumption of circular periodicity [37,38]. In this case, only one tube and the surrounding volume of PCM are considered (see Fig 6). Optimized configurations for a single-tube are then identically replicated for all the tubes, implicitly assuming that entire shell-and-tubes LHTES unit would be optimized as well. To illustrate the key difference between design approaches, we optimized the LHTES with and without the circular periodicity assumption. The optimized configurations for the two cases are presented in Fig 6. The optimized design with the circular periodicity assumption (single-tube design) was found *using topology optimization for only one of the sub domains* identified by the red circles in Fig. 6b. The optimized design without the circular periodicity assumption (multi-tube design) was obtained by performing a topology optimization run for the entire LHTES unit comprising the four pipes.

The results of Fig 6 were obtained for PCM solidification process (discharge) and without considering the gravity force in the momentum equation. No natural convection due to buoyancy takes place under such conditions. This simplification is necessary to ensure circular periodicity. With gravity force included in the model no circular periodicity exists for the problem under investigation since **g** vector acts only along the vertical direction.

The time evolution of liquid fraction field, presented in Fig 7, shows significant differences between the behavior of a globally optimized LHTES unit with respect to the one designed via circular periodicity. For the single-tube design, four solidification fronts advance concentrically until they merge and reach the outer shell as well (t = 0.60). The multi-tube design allows to obtain a more even distribution of liquid fraction, particularly during the late stages of PCM solidification process (t > 0.9). It appears therefore that a global optimization of the geometry is crucial to capture all relevant aspects of the process, even in the conduction dominated case.

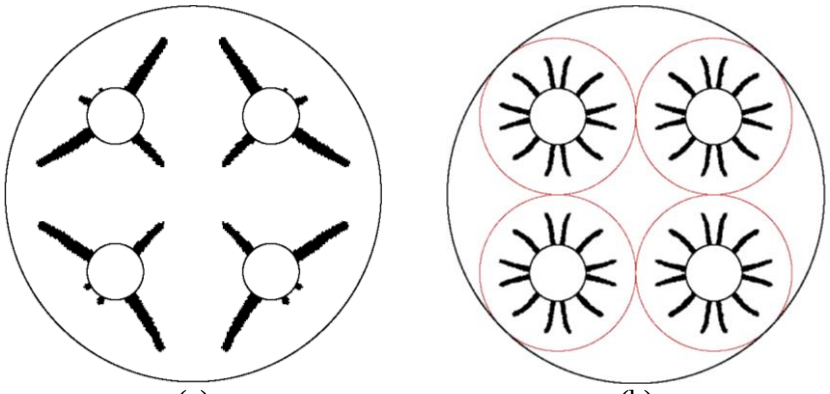

(a) (b)

Figure 6. Optimized designs obtained without (a) and with (b) the circular periodicity assumption. Each of the red circles in (b) indicates the periodic region considered.

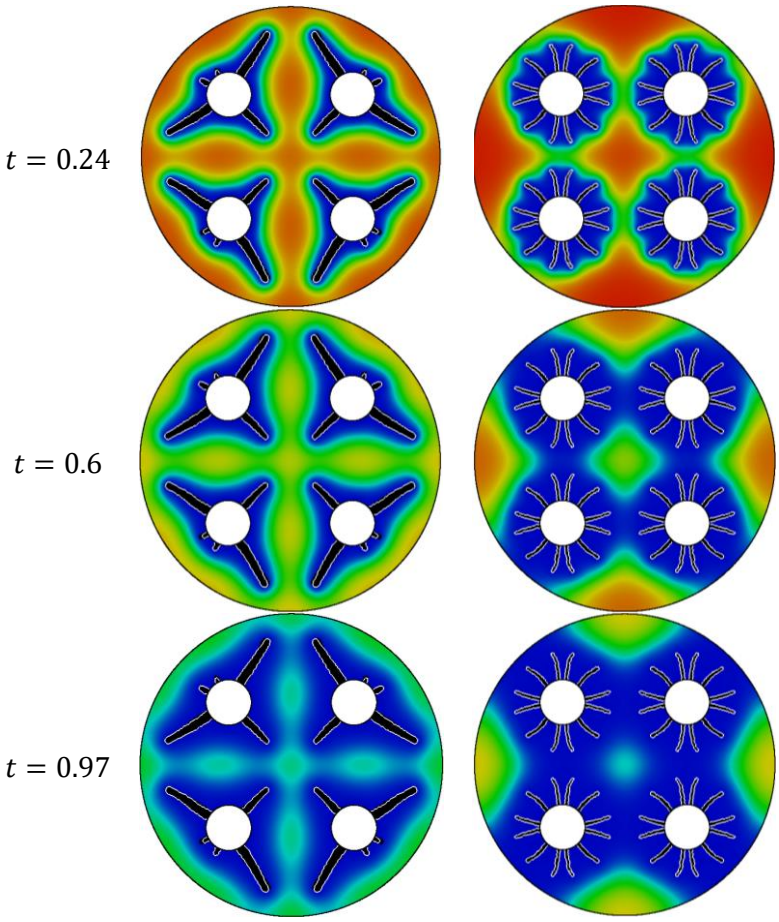

Figure 7. Liquid fraction at selected time instants. Referring to Figure 6, the left column shows design (a), and the right column shows design (b).

The time evolution of the state of charge reported in Fig 8 enables to have a further insight into the difference between the multi-tube design and the single-tube design. Interestingly, the single-tube design produces faster discharge in the case of shallow discharge processes, that is for a final SoC larger than ~ 20%. This is ascribable to the higher overall heat transfer area present in the single-tube design compared with the multi-tube one. Nevertheless, for deep discharge – i.e. a final SoC smaller than ~ 20% – the multi-tube design discharges faster, which indeed is what it was designed for, as detailed in Section 2. This unequivocally shows that the design of TES systems is tightly connected to the storage process and services its aims to provide, here encapsulated in the desired final SoC. Design TES systems that specifically aim at desired functionality and services is therefore essential. This necessity is further stressed under real-life operating conditions, as TES systems are likely to experience variable duty cycles, encompassing for instance both partial and full charge/discharge cycles. We therefore would like to stress to the energy storage community that tailored and possibly robust designs of TES are paramount.

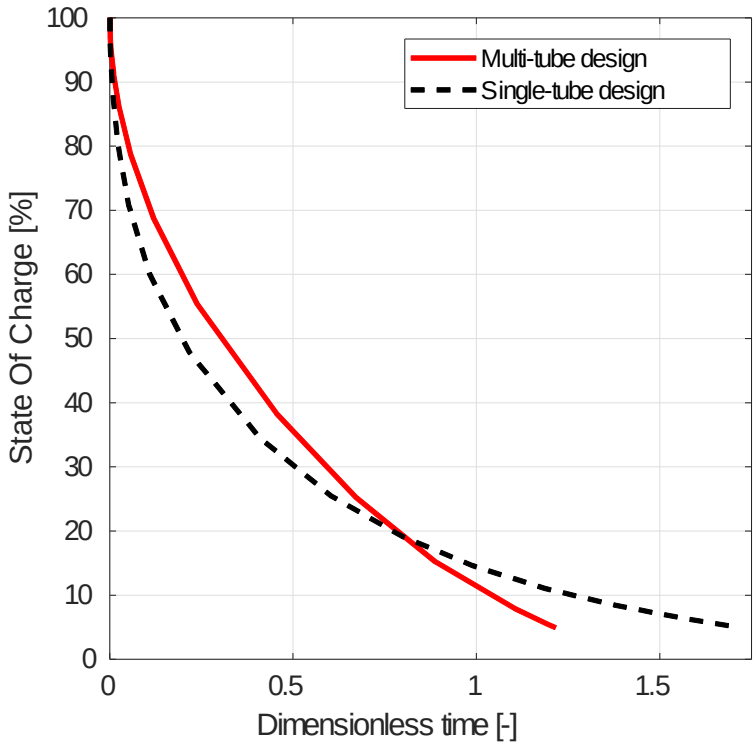

Figure 8. State of Charge history during a discharge process for the full multi-tube and for the periodic single-tube layouts.

3.3. Optimal design of shell-and-tubes LHTES units with separate hydraulic loops for charging and discharging

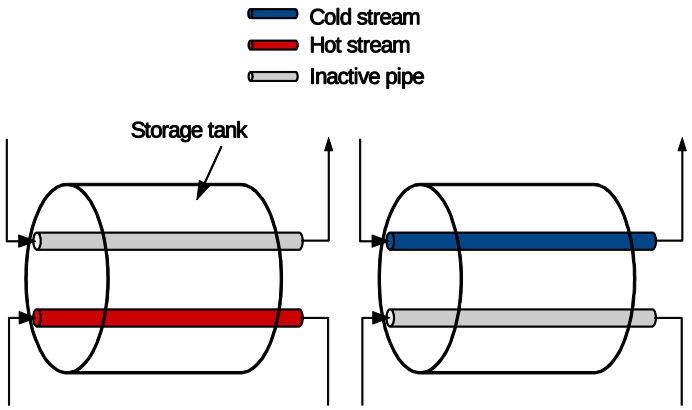

Figure 9. Schematic representation of a multi-tube system with separate loops during charge (left) and discharge (right).

In this section, we describe how the optimized fin configuration should change when the system is operated using separate hydraulic loops. The schematic in Fig 9 illustrates the concept for a shell-and-tubes LHTES unit. During

charging, the HTF flows through a set of tubes (the charging loop) dedicated to transfer thermal energy from the HTF to the PCM (charging process). During this process, a second set of tubes (the discharge loop) is inactive. That is, no HTF flows through them. During the discharging process the reverse condition occurs. The HTF sweeps through the discharge loop to retrieve the energy stored in the LHTES system. The charge loop is now inactive. It is therefore evident that the configuration with separate loops induces a different behavior of the LHTES systems in comparison with the single loop cases previously considered.

The same LHTES unit with four tubes adopted in the previous sections was still considered, but with the bottom pair of tubes acting as charge hydraulic loop and the upper pair as discharge hydraulic loop. Topology optimization was then carried out considering the LHTES unit operating according to the duty cycle illustrated in Fig 10. The cycle consists of a charging process followed by a discharging process. Such a choice it is obviously dictated by the fact that the hydraulic loops operate at different stages, the bottom pipes during charging with the upper pair of pipes inactive, and vice versa during discharging. To obtain the optimal configuration of the LHTES with separate loops it is therefore necessary to capture the entire operation of all the pipes, hence the need to consider a charge plus discharge duty cycle.

Furthermore, two extra cases were considered for comparison purposes: i) a *single* hydraulic loop LHTES optimized only for charging and ii) a *single* hydraulic loop LHTES optimized only for discharging. Such cases where then compared with the optimized LHTES system with separate hydraulic loops.

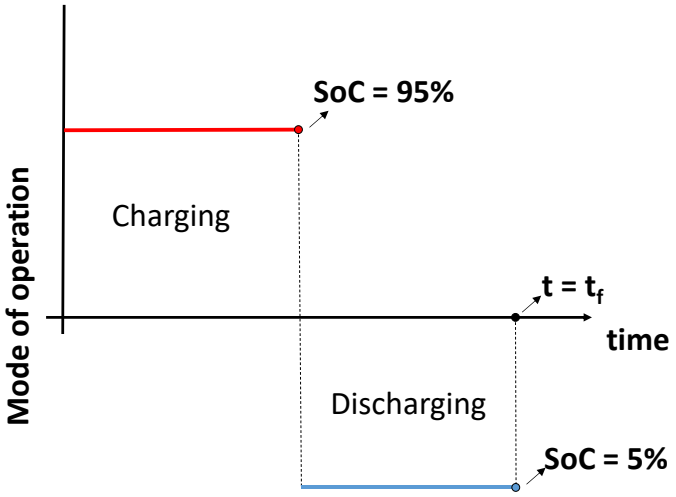

Figure 10. Schematic duty cycle considered for the topology optimization of multi-tube LHTES with separate hydraulic loops.

In all the studies presented in the previous sections, a time-independent Dirichlet condition (Eq. 6) was prescribed to all the tubes within the shell. Hence, the effect of the HCM of which the pipe is made could be neglected. However, in the present study, the Dirichlet condition is imposed only to the bottom tubes for charging and only to the top tubes for discharging. The inactive tubes (the top tubes for charging and the bottom tubes for discharging) contribute to heat transfer enhancement due to the HCM covering their surface. To account for this effect, here we considered a fixed HCM layer of thickness $dr = 0.02$ over Γ_d.

Figure 11a illustrates the optimized LHTES design for separate hydraulic loops alongside the ones optimized for a single hydraulic loop operation. The difference between such configurations is striking. When separate loops are considered, together with the duty cycle of Fig 10, the optimized fins transform into two continuous branches connecting the bottom and upper tubes (Fig 11). This feature allows the full utilization of the highly conductive

material in the LHTES unit and it ensures that the material is best utilized during both charging and discharging, which occur at different times and by operating two separate pairs of tubes (i.e. separate hydraulic loops).

A look at the time evolution of the liquid fraction field for charging (Fig 12) and discharging (Fig 13) allows to interpret why a design with connected pipes (Fig. 11a) emerged. Due to separate hydraulic loops, during charging the HTF passes only through the bottom pipes. As a result, liquid PCM starts to form only in the proximity of such pipes in the lower region of the LHTES unit. The vertical branches provide then an enhancement of heat transfer in vertical direction, shifting upwards the melting front. This can be already observed at the beginning of charging ($t = 0.74$), where the liquid PCM has already reached the upper tubes and it becomes more evident at later times. The two branches therefore allow to thermally connect the bottom pipes with the upper region where most of the solid PCM is found by facilitating the upwards movement of the melting front. If designs optimized for a single-loop configuration are used, the large heat transfer area obtained through their optimized layout with branched fins yields a quick melting of the bottom region of the shell during the initial part of the process (Fig. 12 at $t = 0.74$). However, the heat transfer rate drops quickly when $t > 0.74$ as most of the solid PCM is located far away from the heated pipe.

It is crucial, however, to recall that the design with connected pipes (Fig 11a) *is the solution optimized for the entire duty cycle* illustrated in Fig 10, namely for a charge followed by a discharge. It is therefore essential to also investigate the liquid fraction evolution during the discharge process. During discharge (Fig. 13) solidification begins around the upper pipes, since the bottom pipes are inactive. In this case, the vertical branches provide heat transfer enhancement by promoting the advancement of the solidification front along the downward direction, as evident from Fig 13a. In fact, already at $t = 0.99$ solid PCM surrounds both pairs of tubes, although only the upper ones are active during discharge. Therefore, the vertical branches connect thermally the upper pipes (active during discharge) with the lower part of the LHTES unit, where there is most of the liquid PCM. On the other hand, the solidification front advances slowly towards the bottom of the shell in the layouts optimized for a single-loop configuration.

The results above suggest that the two thick branches provide heat transfer enhancement for both the charging and discharging processes that *compound* the duty cycle (Fig. 10). During charging the branches facilitate the upward movement of the melting front departing from the bottom pipes The branches *also* enhance the discharge process by favoring the advancement of the solidification front from the upper pipes toward the lower part of the LHTES system. Therefore, the optimized design enhances melting without penalizing excessively solidification *and vice versa*.

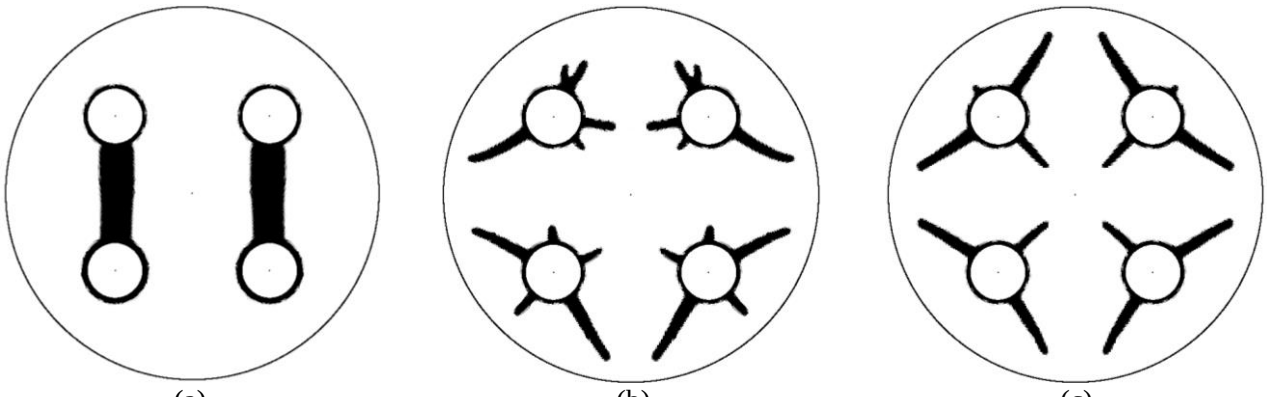

Figure 11. (a): Optimized designs of a unit with separate hydraulic loops; (b): optimized design of a single-loop unit for fastest charge; (c): optimized design of a single-loop unit for fastest discharge.

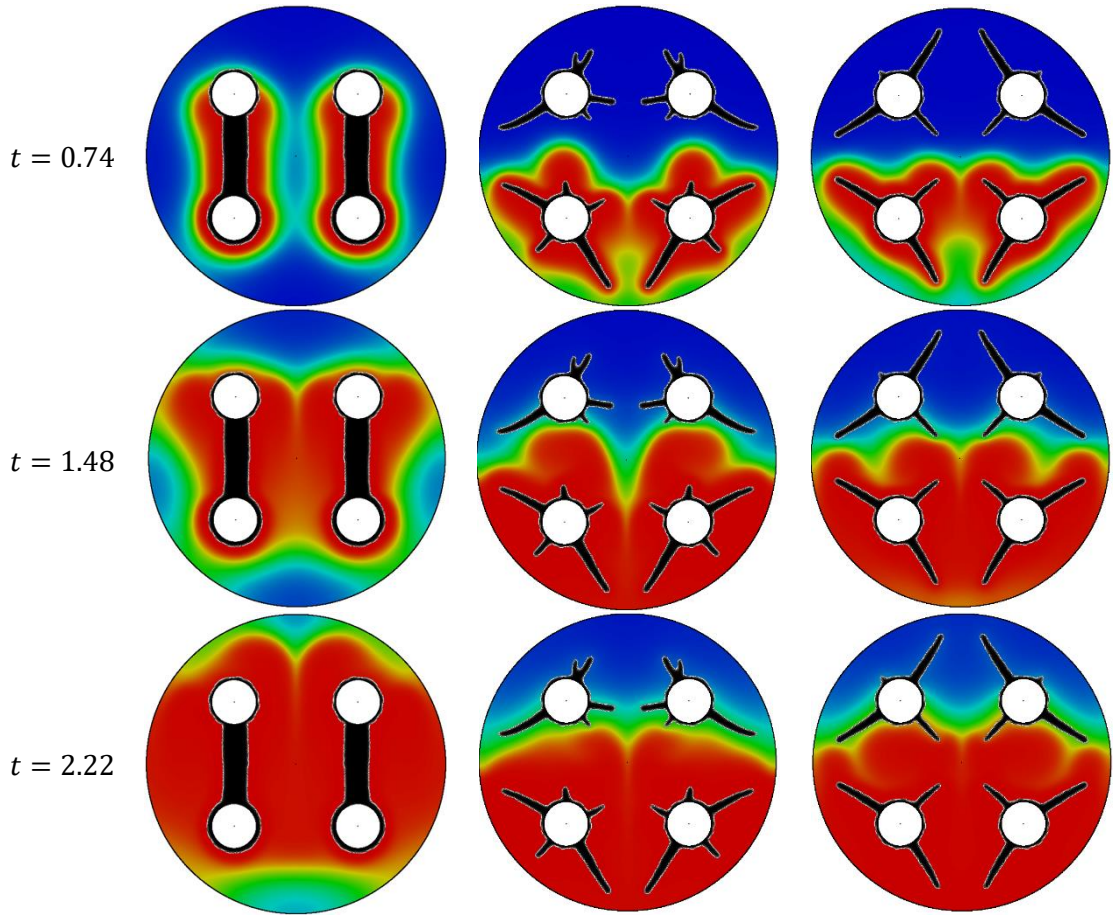

Figure 12. Liquid fraction at selected time instants during melting. Referring to Figure 11, the left column shows design (a), the central column shows design (b), the right column shows design (c)

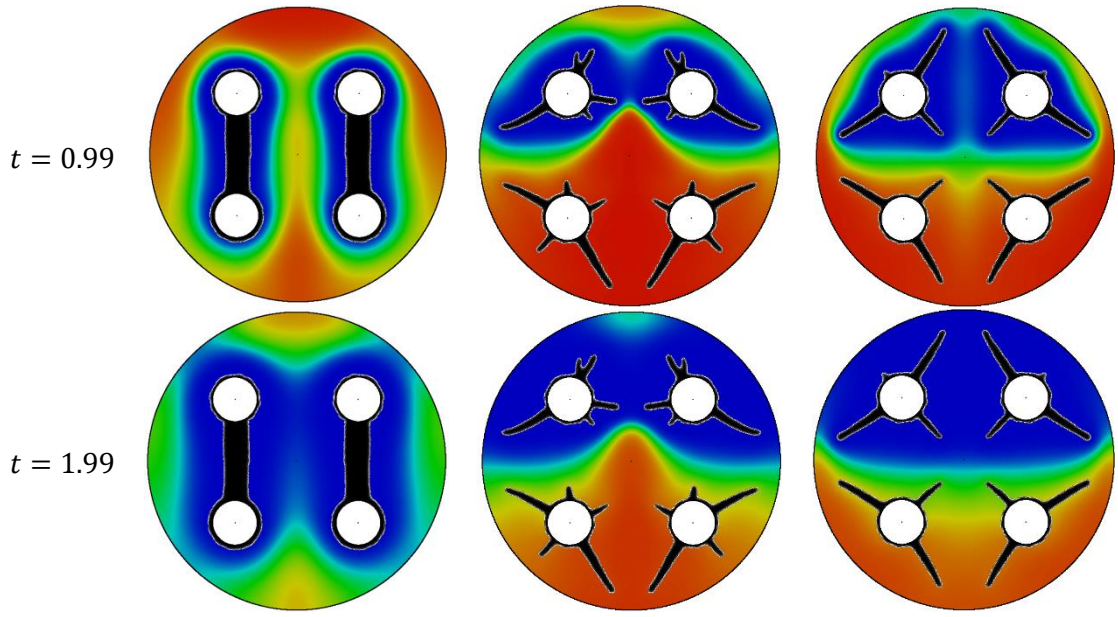

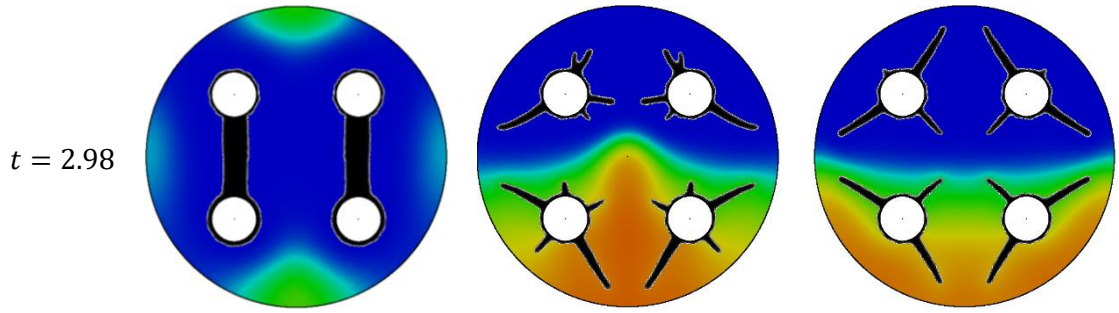

Figure 13. Liquid fraction at selected time instants during solidification. Referring to Figure 11, the left column shows design (a), the central column shows design (b), the right column shows design (c)

3.4. Effect of fins material-PCM pair selection on charge and discharge time of optimized LHTES units

As illustrated in Section 3.1, the combined effect of the thermophysical properties of PCM and fins material (i.e. HCM) significantly affects the optimized design. In particular, for a fixed amount of HCM, the optimized configurations span from conduction-dominated to convection-dominated designs, depending on the PCM-to-HCM thermal diffusivity ratio, C_k. It is however crucial to recognize that, for a given application of a LHTES unit, the selection of the PCM is strongly affected by the intended operating temperature, which in turn vastly dictates the melting point of the PCM and thus the class of PCM itself [39]. Therefore, the selection of the fins material is commonly done in the light of a mandatory choice of a PCM that fits the intended application (i.e. the operating temperature). Under such constraints, it remains open the question of which HCM should be selected to enhance a particular PCM. Furthermore, it is not clear whether this material selection could be done a priori, without knowing the optimized fin geometry. Such questions and their impact on the performance of a multi-tube LHTES unit are addressed in this section.

Aluminum, graphite, stainless steel and copper were considered as materials for the fins (see Table 1). Three materials were selected as potential PCMs: PCM 11, a salt hydrate for cooling applications; RT100, a commercial paraffin wax for mid temperature applications; SS, a binary molten salt eutectic, commonly referred to as solar salt, for mid/high temperature applications. Table 2 lists the main properties of such PCMs. Given a PCM type among the three considered, two topology optimization runs (one for charging and one for discharging) were carried out for each fins material and the results were compared to identify the best fins material-PCM pairs. Therefore, a total of 24 topology optimization runs were performed (4 fins materials x 3 PCMs x 2 processes).

Table 1
Fins materials

Property	Graphite foil	Aluminum	Stainless steel	Copper	Ref
C_{mat} - Cost per unit volume [k$/m3]	10	7	20	40	[40][41]
C_m - Cost per unit mass [k$/kg]	10	2.59	2.56	4.45	[40][41]
Φ_{MAX} - Maximum volume fraction [-]	0.07	0.1	0.035	0.0175	

Table 2
Thermo-physical properties of PCMs

Property	PCM-11	SS	RT100
Melting temperature [°C]	-11	230	100
Latent heat [kJ/kg]	250	110	140
Thermal conductivity [W/(m K)]	1.25	0.5	0.2
Specific heat [kJ/(kg K)]	2.5	1.6	2
Density [kg/m3]	1130	2000	800

Reference	[42]	[43]	[24]

In order to adequately investigate the effect of fins material-PCM pair selection, the constraints in the topology optimization framework illustrated in Section 2 were slightly modified. In particular, a different maximum volume fraction Φ_{MAX} [1] (see Eq. 1) for the fins was considered for each type of fins material, as reported in Table 1. Each Φ_{MAX} was determined in order to ensure that the maximum total cost C_{TOT} *for the fin material* remained the same in each case considered. The maximum total cost $C_{TOT}$was estimated as the product of the maximum volume fraction, the volume of the unit and its specific cost per unit volume. That is, $C_{TOT} = \Phi_{MAX} \times V \times c_{mat}$. Although this estimation accounts only for the commodity costs, but not for example manufacturing, it provides a meaningful constraint to perform a meaningful comparison of the different pairs of fins material-PCM combination. If fact, the opposite situation with a Φ_{MAX} identical for each case would lead to the trivial conclusion that the fins should be always made out of the material with the largest thermal conductivity/thermal diffusivity. This is clearly not representative of a typical engineering design process for LHTES units, in which the designer is confronted with the question of finding the optimal shape of fins, the corresponding material and its amount under cost constraints. Therefore, although a first approximation of costs, the condition $C_{TOT} = \Phi_{MAX} \times V \times c_{mat} = constant$ is representative and necessary to properly address the question posed, as also corroborated by the results illustrated thereafter. It is also worth to mention why the cost of PCM was not considered in a similar manner. As mentioned above and reiterated here, we considered that the PCM choice was dictated by the intended application through the necessary operating temperature (i.e. melting point). Specifically, an application for each PCM: cooling (PCM11, T_m = -11°C), mid temperature application (RT100, T_m = 100°C) and high temperature application (SS, T_m = 230°C). Therefore, the PCM choice in the context of this work was subject to matching the necessary application rather than costs.

Figure 14 summarizes the outcomes of the topology optimizations carried out. For each PCM type – hence for each TES application – two rectangles that identify the range of energy density and charge/discharge times are drawn. Each rectangle encapsulates the outcomes (different markers) for each PCM-fins material pair, *for the given PCM and process*. Each marker within the rectangle therefore pinpoints the performance of the LHTES unit with a certain material for the fins, enabling to cross compare performances and select the most suitable material for the fins.

It is important to note that for each PCM the energy density spans across a small range, identified by the height of each rectangle reported in Fig 14. This can be easily explained by reconsidering that the maximum volume fraction Φ_{MAX} of the fins is different for each material, as reported in Table 1. A higher Φ_{MAX}, implies less volume available for PCM, hence a reduction in the energy density. This is evident from Fig 14 where a LHTES unit with aluminum fins has the lowest energy density for a given PCM. In fact, referring to Table 1, Φ_{MAX} for aluminum is the highest one. Nevertheless, for each PCM type the energy density remains within a range of ~10%, rendering the comparison of the results still meaningful.

The order of markers in Fig 14 elucidates what is the favorable material for fins. Firstly, the order shows once again that discharge process is slower than charging. This is not surprising as charging process benefits from intrinsic heat transfer enhancement due to natural convection, as discussed in Section 3.1. More importantly, it is evident that optimized fins made of aluminum achieve fastest charging/discharging for each one of the PCMs considered, i.e. maximum heat transfer enhancement is achieved in this case. Graphite is a close contender, but still it falls short to aluminum even though its thermal diffusivity is more than 2-fold larger. It is relevant also to notice that fins made out of copper are outperformed by both aluminum and graphite. For example, the charging time for RT100 is more than double if fins of copper are employed rather than aluminum ones. A similar trend appears also for SS and for PCM-11. Furthermore, the choice of appropriate fins material seems more important

[1] Φ_{MAX} is defined as the maximum fins volume allowed within the shell of the LHTES unit – see Eq. (1).

in the case of discharging, since the difference in discharging time between aluminum and the other materials is larger than in the charging case. Once more, this is due to the fact that the discharging process is mostly dominated by pure conduction without the benefits of natural convection.

Lastly, stainless steel is the least favorable option since it provides the least enhancement among the four materials considered. This is particularly evident for the RT100 discharge process and to a lesser extent for both charging/discharging of SS and PCM-11.

To conclude this section, it is important to emphasize that the identification of aluminum as most suitable material for fins had been possible only through the optimization approach proposed here complemented with representative constraints. This can be appreciated through Table 4, which ranks the material for the optimized fins. It is noticeable that the ranking could *not* have been inferred neither from key thermal properties (conductivity/diffusivity) nor from amount of fins material employed (volume fraction) or specific costs. This highlights that the pursue of optimal LHTES systems is a coupled design-material challenge, and that these two elements need to be considered simultaneously. Our future work will therefore enrich this analysis by bringing into consideration further attributes such as manufacturability, chemical compatibility/kinetics (e.g corrosion/nucleation/subcooling) and economical details.

Table 4
Ranking of materials for fins in multi-tube LHTES units

Material	Ranking	Charge/Discharge time	Thermal conductivity [40][41]	Thermal diffusivity	Volume fraction	Cost per unit volume [40][41]
Aluminum	1	0.87/0.95	200	82.31	0.1	7
Graphite	2	1.07/1.15	150	214.29	0.07	10
Copper	3	1.97/2.47	350	99.43	0.0175	40
Steel	4	2.00/2.60	20	5.13	0.035	20

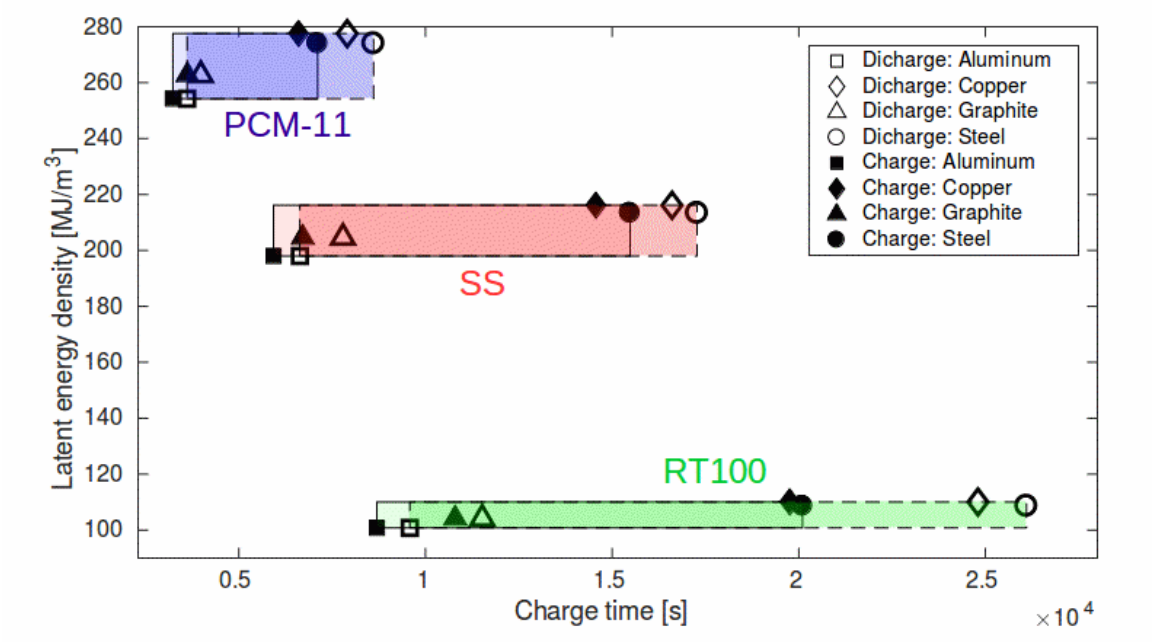

Figure 14. Charge and discharge times of the optimized layouts obtained with different HCM-PCM couplings

4. Fabrication of LHTES units

The fabrication of the fins configurations obtained through topology optimization requires manufacturing methods capable of dealing with the complex geometrical features illustrated, for example, in Fig 2. In this section, we focus on additive manufacturing (3D printing) and examine if the optimized configurations are manufacturable using such fabrication process. The topology optimization results presented in this paper were converted into physical components following the post-processing procedure illustrated by Zegard et al [44]. The method can be summarized in three steps:

1. Threshold the continuous density field in order to isolate the blackest regions as the one corresponding to the fins and add the pipes (Figure 15a). The value of the threshold is obtained to ensure that this operation does not lead to a layout violating the maximum HCM volume constraint.
2. Extrude the geometry obtained in step 1 along the axial direction of the shell (Figure 15b). The extrusion vector magnitude should be set equal to the desired length of the unit. Note that extruded 2D geometries are suboptimal due to: (a) the varying temperature of the HTF along the axial direction and (b) the restriction of the design space (2D instead of 3D) considered in the optimization process. The effect of (b) was already investigated in our previous work [23].
3. Extract the surface enclosing the object obtained in step 2 and triangulate it using a meshing software to obtain a STereoLithography (STL) file for direct manufacturing [44].

Finally, the manufacturability of the STL geometry was assessed using the Formlabs Form 2 Stereolytography 3D printer (Fig 16a) using resin V2. The resin was UV cured layer by layer, downward from the build plate (Fig 16b). The manufactured part is shown in Fig 16 and 17. It can be observed that the geometrical features have been fabricated reasonably well in comparison with the optimized geometry (Fig 2). It is in fact possible to observe the very short bifurcations at the extremity of four fins, as well as the slightly tapered shape of the long fins.

However, an operational LHTES device would require using metallic materials (Section 3.4), and thus 3D printing methods such as selective laser sintering. Furthermore, scalability would need to be considered as well. Nevertheless, the results presented in this section provide the initial evidences and confidence that our topology-optimized geometries have features adequate to be fabricated by additive manufacturing. Metallic 3D printing of the LHTES devices will be fully verified through our ongoing work. Regarding the costs, these are clearly very application dependent and necessitate assessment on case-by-case basis. Nevertheless, topology-optimized LHTES devices have also the potential to inspire simplified geometries, as we illustrated in [15], that can be fabricated with conventional methods.

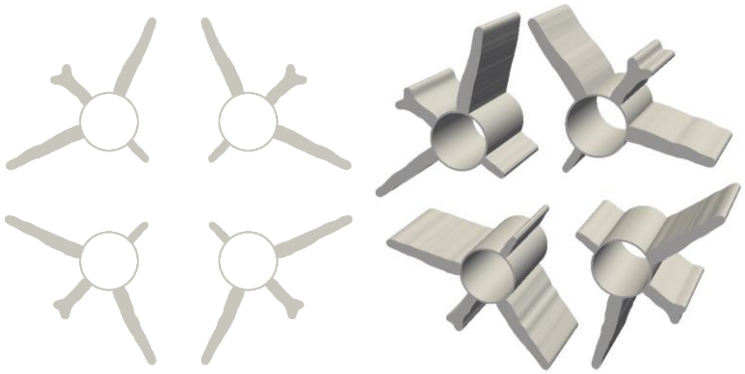

Figure 15. Post-processing numerical results into real-world LHTES units. (a): threshold geometry; (b): extruded geometry

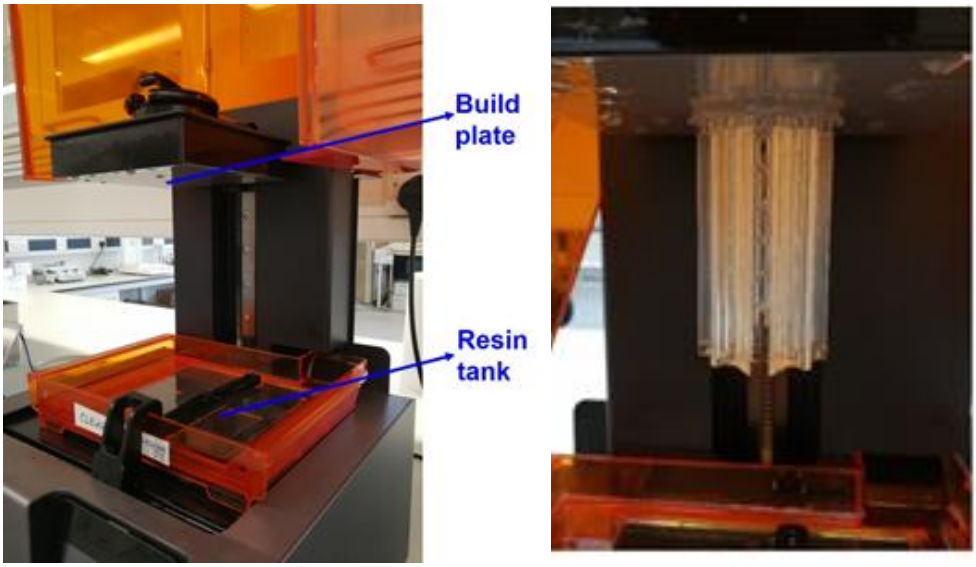

Figure 16. Stereolytography 3D printer (left) and the built geometry hanging from the build plate (right)

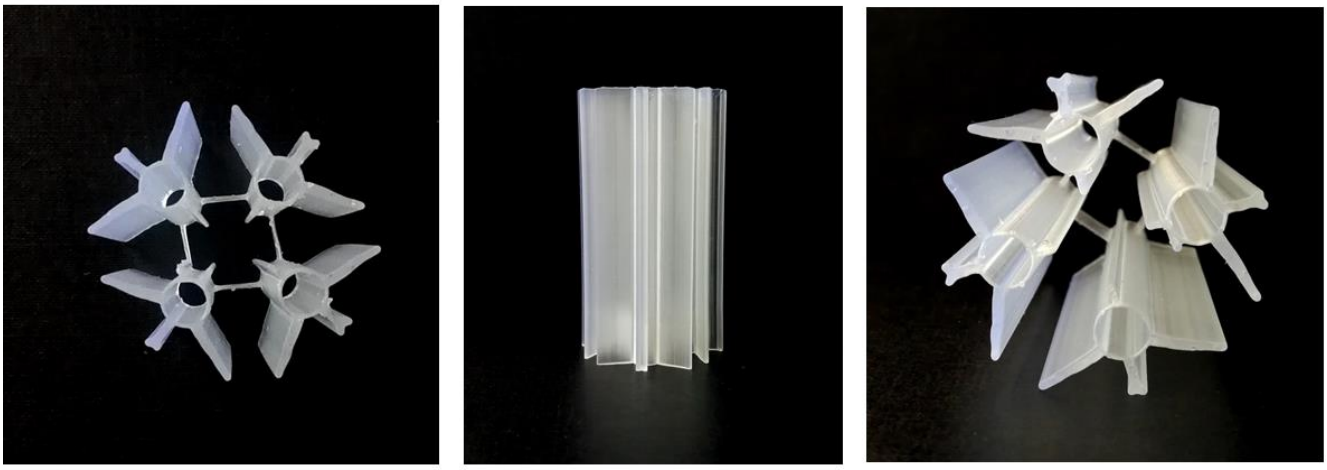

Figure 17. 3D printed multi-tube LHTES unit with the optimized fins configuration.

5. Conclusions

In this paper, we have presented optimized configurations of horizontal multi-tube latent heat thermal energy storage (LHTES) systems under multiple operating conditions, flow arrangements and design constraints. The topology optimization method was used to obtain the optimized designs and reach the following conclusions:

- The ratio of PCM to fins material thermal diffusivity, $C_{k,}$ affects the behavior of the multi-tube LHTES unit, leading to either units dominated by heat conduction or natural convection. The results show that the optimized topology of the fins changes accordingly. For $C_k > 2\%$, asymmetrical fins start to emerge due to intrinsic enhancement of heat transfer caused by natural convection currents. Establishing this design-physics link was possible due to the design freedom enabled by the topology optimization method adopted in this work.
- Multi-tube LHTES units with fins optimized by considering only one pipe in the design process (i.e. 'periodicity assumption') might lead to suboptimal configurations of the entire unit. The results presented show that a LHTES unit whose fins are optimized considering simultaneously all the pipes performs better

when a deep discharge process is addressed. On the other hand, the design found under the periodicity assumption shows a faster discharge rate during early stages of the process. This illustrates two key elements: i) the periodicity assumption – commonly adopted in the literature – should be used cautiously; ii) the design of LHTES systems is tightly connected to the storage process and services its aims to provide (for example, deep discharge vs shallow discharge). The extent to which designs are specifically tailored to one or more desired operations should be carefully considered.

- The optimized fin layout drastically varies when separate flow passages (hydraulic loops) are considered for charging and discharging process. The numerical studies presented in this paper suggest that fins connecting the two hydraulic loops (pairs of tubes) are convenient for a complete charging-discharging cycle. In fact, such unconventional configuration promotes both melting (charging) as well as solidification (discharging).
- The fin material should be chosen in parallel with the layout of the fins when a maximum cost constraint is considered. For a given PCM type (salt hydrate, paraffin wax, molten salt), we found that optimized fins made of aluminum outperform other fins materials with higher thermal conductivity. This highlights that the optimization of LHTES systems is a co-design challenge, in which geometry and material choice should be addressed in parallel.
- 3D printing was demonstrated to be a suitable to manufacture the topology-optimized designs of multi-tube LHTES systems.

In summary, we have presented novel designs of multi-tube LHTES systems obtained via topology optimization and how their optimized configurations are tightly connected to the underlying heat transfer phenomena. Future work is necessary to include economic constraints, manufacturability requirements and storage cycles in the design framework. Furthermore, high-porosity metal foams and matrices are being intensively considered for heat transfer enhancement in LHTES units, as they guarantee minimal impact on the total storage capacity. For this reason, developing novel design methods able to yield high-performance HCM structures optimized at both the microscopic and macroscopic scales deserves attention for future research.

Acknowledgments

Dr. A. Sciacovelli acknowledges the financial support from Engineering and Physical Sciences Research (EPSRC) Council, UK (EP/R016402/1)

References

[1] Shifrin C. The heat is on. Nat Energy 2016;22:28–9. doi:10.1038/nphys2638.

[2] HM Government. The Clean Growth Strategy: Leading the way to a low carbon future 2017:165.

[3] DECC. The Future of Heating: A strategic framework for low carbon heat in the UK. Dep Energy Clim Chang 2012:1–120.

[4] Crespo A, Barreneche C, Ibarra M, Platzer W. Latent thermal energy storage for solar process heat applications at medium-high temperatures – A review. Sol Energy 2018:1–32. doi:10.1016/j.solener.2018.06.101.

[5] Du K, Calautit J, Wang Z, Wu Y, Liu H. A review of the applications of phase change materials in cooling, heating and power generation in different temperature ranges. Appl Energy 2018;220:242–73. doi:10.1016/j.apenergy.2018.03.005.

[6] Brückner S, Liu S, Miró L, Radspieler M, Cabeza LF, Lävemann E. Industrial waste heat recovery technologies: An economic analysis of heat transformation technologies. Appl Energy 2015;151:157–67. doi:10.1016/j.apenergy.2015.01.147.

[7] Johnson M, Hübner S, Braun M, Martin C, Fiß M, Hachmann B, et al. Assembly and attachment methods for extended aluminum fins onto steel tubes for high temperature latent heat storage units. Appl Therm Eng 2018;144:96–105. doi:10.1016/j.applthermaleng.2018.08.035.

[8] Riahi S, Saman WY, Bruno F, Belusko M, Tay NHS. Performance comparison of latent heat storage systems comprising plate fins with different shell and tube configurations. Appl Energy 2018;212:1095–106. doi:10.1016/j.apenergy.2017.12.109.

[9] Tay NHS, Belusko M, Castell A, Cabeza LF, Bruno F. An effectiveness-NTU technique for characterising a finned tubes PCM system using a CFD model. Appl Energy 2014;131:377–85. doi:10.1016/j.apenergy.2014.06.041.

[10] Sciacovelli A, Gagliardi F, Verda V. Maximization of performance of a PCM latent heat storage system with innovative fins. Appl Energy 2015;137:707–15. doi:10.1016/j.apenergy.2014.07.015.

[11] van Alebeek R, Scapino L, Beving MAJM, Gaeini M, Rindt CCM, Zondag HA. Investigation of a household-scale open sorption energy storage system based on the zeolite 13X/water reacting pair. Appl Therm Eng 2018;139:325–33. doi:10.1016/j.applthermaleng.2018.04.092.

[12] Arena S, Casti E, Gasia J, Cabeza LF, Cau G. Numerical analysis of a latent heat thermal energy storage system under partial load. Renew Energy 2018. doi:10.1016/j.renene.2018.05.072.

[13] Elbahjaoui R, El Qarnia H. Numerical Study of a Shell-and-Tube Latent Thermal Energy Storage Unit Heated by Laminar Pulsed Fluid Flow. Heat Transf Eng 2017;38:1466–80. doi:10.1080/01457632.2016.1255083.

[14] Zheng ZJ, Xu Y, Li MJ. Eccentricity optimization of a horizontal shell-and-tube latent-heat thermal energy storage unit based on melting and melting-solidifying performance. Appl Energy 2018;220:447–54. doi:10.1016/j.apenergy.2018.03.126.

[15] Pizzolato A, Sharma A, Maute K, Sciacovelli A, Verda V. Design of effective fins for fast PCM melting and solidification in shell-and-tube latent heat thermal energy storage through topology optimization. Appl Energy 2017;208:210–27. doi:10.1016/j.apenergy.2017.10.050.

[16] Sciacovelli A, Colella F, Verda V. Melting of PCM in a thermal energy storage unit: Numerical investigation and effect of nanoparticle enhancement. Int J Energy Res 2013;73:1610–23. doi:10.1002/er.2974.

[17] Tay NHS, Belusko M, Castell A, Cabeza LF, Bruno F. An effectiveness-NTU technique for characterising a finned tubes PCM system using a CFD model. Appl Energy 2014;131:377–85. doi:10.1016/j.apenergy.2014.06.041.

[18] Belusko M, Halawa E, Bruno F. Characterising PCM thermal storage systems using the effectiveness-NTU approach. Int J Heat Mass Transf 2012;55:3359–65. doi:10.1016/j.ijheatmasstransfer.2012.03.018.

[19] Al-abidi A a., Bin Mat S, Sopian K, Sulaiman MY, Mohammed AT. CFD applications for latent heat thermal energy storage: a review. Renew Sustain Energy Rev 2013;20:353–63. doi:10.1016/j.rser.2012.11.079.

[20] Wang P, Yao H, Lan Z, Peng Z, Huang Y, Ding Y. Numerical investigation of PCM melting process in sleeve tube with internal fins. Energy Convers Manag 2016;110:428–35. doi:10.1016/j.enconman.2015.12.042.

[21] Sciacovelli A, Navarro ME, Jin Y, Qiao G, Zheng L, Leng G, et al. High density polyethylene (HDPE)-Graphite composite manufactured by extrusion: A novel way to fabricate phase change materials for thermal energy storage. Particuology 2017;40:131–40. doi:10.1016/j.partic.2017.11.011.

[22] Mahdi JM, Lohrasbi S, Ganji DD, Nsofor EC, Jasim M. Mahdi, Sina Lohrasbi, et al. Accelerated melting of PCM in energy storage systems via novel configuration of fins in the triplex-tube heat exchanger. Int J Heat Mass Transf 2018;124:663–76. doi:10.1016/j.ijheatmasstransfer.2018.03.095.

[23] Pizzolato A, Sharma A, Maute K, Sciacovelli A, Verda V. Topology optimization for heat transfer enhancement in Latent Heat Thermal Energy Storage. Int J Heat Mass Transf 2017;113:875–88. doi:10.1016/j.ijheatmasstransfer.2017.05.098.

[24] Colella F, Sciacovelli A, Verda V. Numerical analysis of a medium scale latent energy storage unit for district heating systems. Energy 2012;45:397–406. doi:10.1016/j.energy.2012.03.043.

[25] Yang X, Lu Z, Bai Q, Zhang Q, Jin L, Yan J. Thermal performance of a shell-and-tube latent heat thermal energy storage unit: Role of annular fins. Appl Energy 2017;202:558–70. doi:10.1016/j.apenergy.2017.05.007.

[26] Ismail KAR, Lino FAM, Da Silva RCR, De Jesus AB, Paixão LC. Experimentally validated two dimensional numerical model for the solidification of PCM along a horizontal long tube. Int J Therm Sci 2014;75:184–93. doi:10.1016/j.ijthermalsci.2013.08.008.

[27] Sigmund O, Maute K. Topology optimization approaches A comparative review 2013. doi:10.1007/s00158-013-0978-6.

[28] Bendsoe MP. Optimal shape design as a material distribution problem. Struct Optim 1989;1:193–202.

[29] Zhou M. The COC algorithm, Part II : Topological, geometrical and generalized shape optimization. Comput Methods Appl Mech Eng 89 1991;89:309–36.

[30] Lazarov BS, Sigmund O, Meyer KE, Alexandersen J. Experimental validation of additively manufactured optimized shapes for passive cooling. Appl Energy 2018;226:330–9. doi:10.1016/j.apenergy.2018.05.106.

[31] Soprani S, Haertel JHK, Lazarov BS, Sigmund O, Engelbrecht K. A design approach for integrating thermoelectric devices using topology optimization. Appl Energy 2016;176:49–64. doi:10.1016/j.apenergy.2016.05.024.

[32] Mitchell SL, Ortiz M. Computational multiobjective topology optimization of silicon anode structures for lithium-ion batteries. J Power Sources 2016;326:242–51. doi:10.1016/j.jpowsour.2016.06.136.

[33] Svanberg K. A class of globally convergent optimization methods based on conservative convex separable approximations. SIAM J OPTIM 2002;12:555–73.

[34] Wang F, Lazarov BS, Sigmund O. On projection methods, convergence and robust formulations in topology optimization. Struct Multidiscip Optim 2011;43:767–84. doi:10.1007/s00158-010-0602-y.

[35] Gresho PM, Sani RL. Incompressible flow and the finite element method advection diffusion and isothermal laminar flow. John Wiley & Sons, Inc.; 1998.

[36] Guelpa E, Sciacovelli A, Verda V. Entropy generation analysis for the design improvement of a latent heat storage system. Energy 2013;53:128–38. doi:10.1016/j.energy.2013.02.017.

[37] Mostafavi Tehrani SS, Taylor RA, Nithyanandam K, Shafiei Ghazani A. Annual comparative performance and cost analysis of high temperature, sensible thermal energy storage systems integrated with a concentrated solar power plant. Sol Energy 2017;153:153–72. doi:10.1016/j.solener.2017.05.044.

[38] Bhagat K, Prabhakar M, Saha SK. Estimation of thermal performance and design optimization of finned

multitube latent heat thermal energy storage. J Energy Storage 2018;19:135–44. doi:10.1016/j.est.2018.06.014.

[39] Xu H, Romagnoli A, Sze JY, Py X. Application of material assessment methodology in latent heat thermal energy storage for waste heat recovery. Appl Energy 2017;187:281–90. doi:10.1016/j.apenergy.2016.11.070.

[40] Callister W, Rethwisch D. Materials science and engineering: an introduction. vol. 94. 2007. doi:10.1016/0025-5416(87)90343-0.

[41] Askeland R. The Science and Engineering of Materials. Cengage Learning, Inc; 2010.

[42] Tay NHS, Bruno F, Belusko M. Comparison of pinned and finned tubes in a phase change thermal energy storage system using CFD. Appl Energy 2013;104:79–86. doi:10.1016/j.apenergy.2012.10.040.

[43] Fornarelli F, Camporeale SM, Fortunato B, Torresi M, Oresta P, Magliocchetti L, et al. CFD analysis of melting process in a shell-and-tube latent heat storage for concentrated solar power plants. Appl Energy 2016;164:711–22. doi:10.1016/j.apenergy.2015.11.106.

[44] Zegard T, Paulino GH. Bridging topology optimization and additive manufacturing. Struct Multidiscip Optim 2016;53:175–92. doi:10.1007/s00158-015-1274-4.